NASA Technical Memorandum 4182

Simplified Model for Solar Cosmic Ray Exposure in Manned Earth Orbital Flights

John W. Wilson, Govind S. Khandelwal,
Judy L. Shinn, John E. Nealy,
Lawrence W. Townsend, and Francis A. Cucinotta

MAY 1990

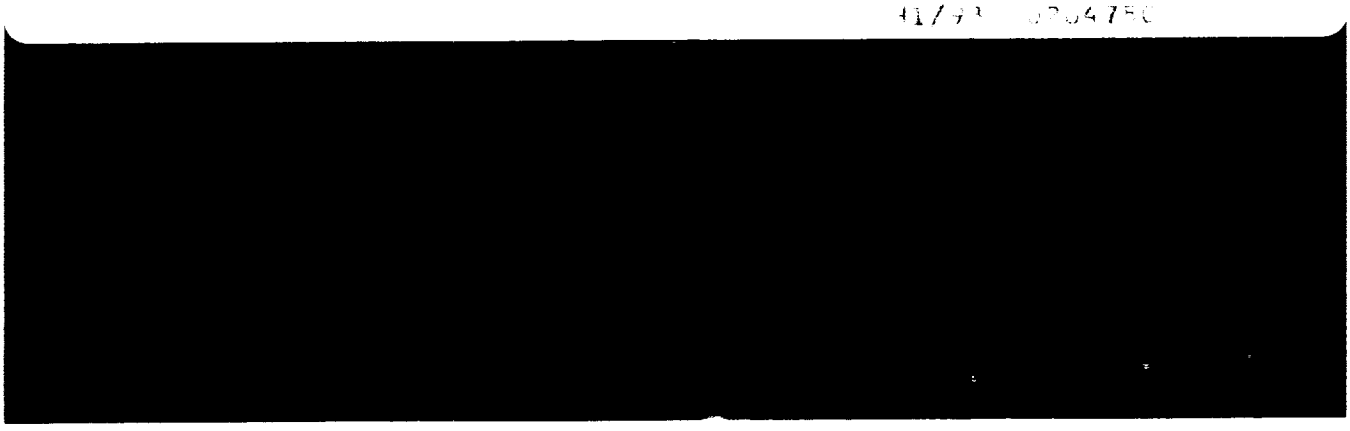

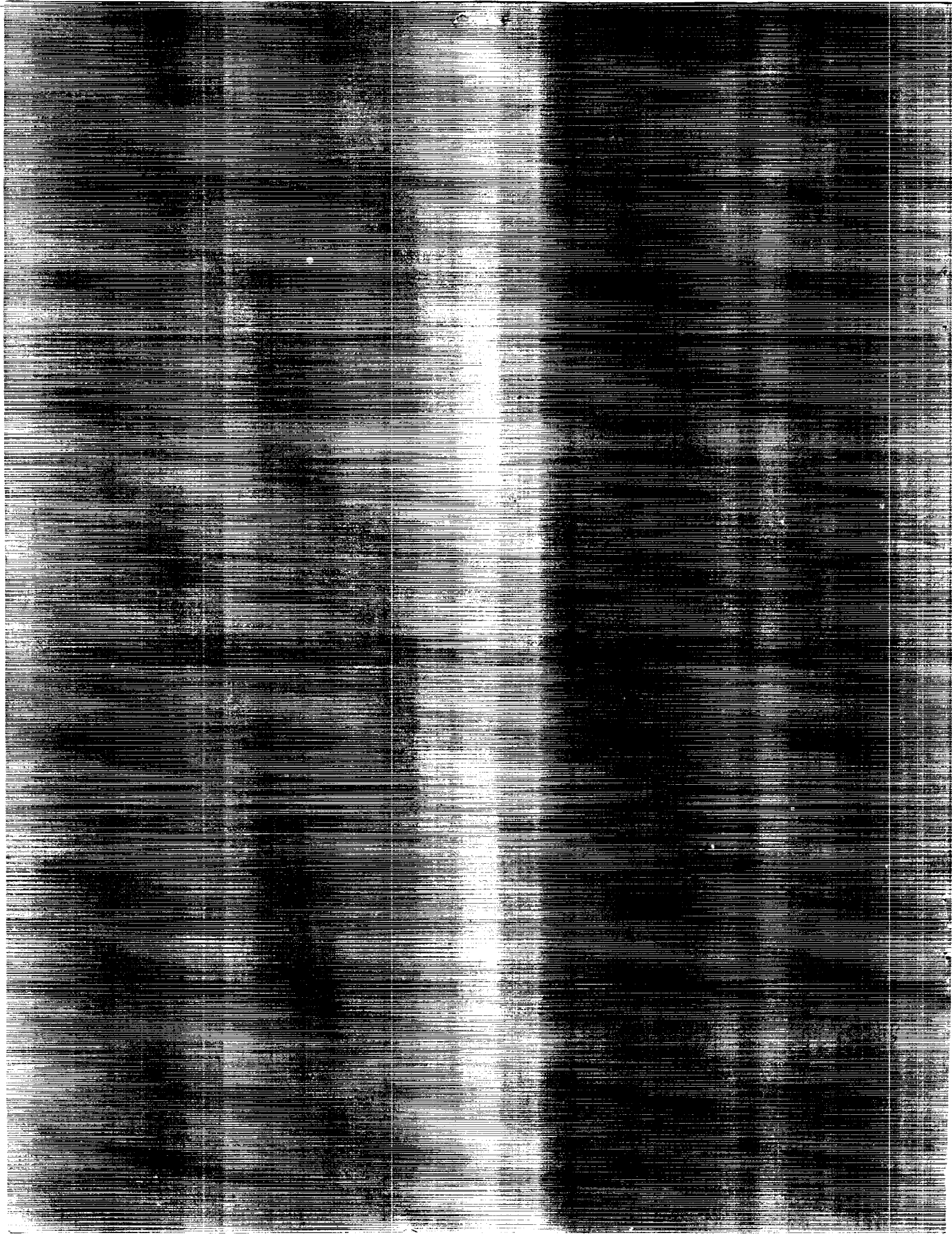

NASA Technical Memorandum 4182

Simplified Model for Solar Cosmic Ray Exposure in Manned Earth Orbital Flights

John W. Wilson
Langley Research Center
Hampton, Virginia

Govind S. Khandelwal
Old Dominion University
Norfolk, Virginia

Judy L. Shinn, John E. Nealy,
and Lawrence W. Townsend
Langley Research Center
Hampton, Virginia

Francis A. Cucinotta
Rockwell International
Space Transportation Systems Division
Houston, Texas

National Aeronautics and
Space Administration
Office of Management
Scientific and Technical
Information Division

1990

Abstract

A simple calculational model is derived for use in estimating solar cosmic ray exposure to critical body organs in low Earth orbit at the center of a large spherical shield of fixed thickness. The effects of the Earth's geomagnetic field, including storm conditions and the astronauts' self-shielding, are evaluated explicitly. The magnetic storm model is keyed to the planetary magnetic index K_p.

Introduction

Solar cosmic rays observed in low Earth orbit first passed through the Earth's magnetic field. Those particles able to penetrate the geomagnetic field must further penetrate the walls of a spacecraft before exposing human occupants. As a result of interactions in the vehicle structure and the bulk tissues of the astronauts' bodies, the composition of the rays is greatly altered. Any reasonable estimate must account for geomagnetic effects, the atomic and nuclear interactions, and the spacecraft and human body geometry.

During years of increased solar activity, varying amounts of the solar plasma are ejected into interplanetary space. When this plasma interacts with the Earth's magnetic field, large distortions of this field result in geomagnetic storms. Since the energetic solar flare particles often arrive during such geomagnetic disturbances, the penetration of the energetic protons into the magnetospheric cavity can be vastly different from that seen under quiet conditions. A magnetic storm model is presented herein to evaluate these effects.

The computational capability existing currently at the National Aeronautics and Space Administration to estimate the absorbed dose for the human occupants in a spacecraft, accounting for all of the aforementioned effects, has been described in reference 1. The computational flow diagram shown in figure 1 of reference 1 depicts the fact that it takes several sequences to obtain dose estimation. Although such detailed dose estimation is more accurate, a simplified straightforward calculational tool is needed for the real-time assessment during space missions. The present effort is to develop a simplified model that integrates all the computational steps and yet provides reasonable accuracy in estimating dose during manned orbital flights.

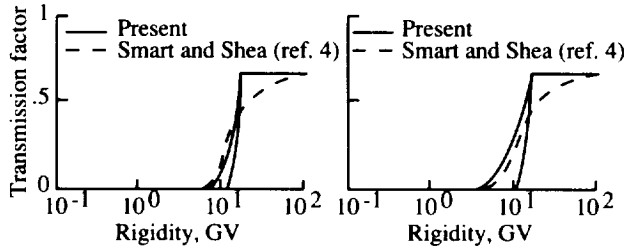

(a) Orbit inclination, 20°. (b) Orbit inclination, 30°.

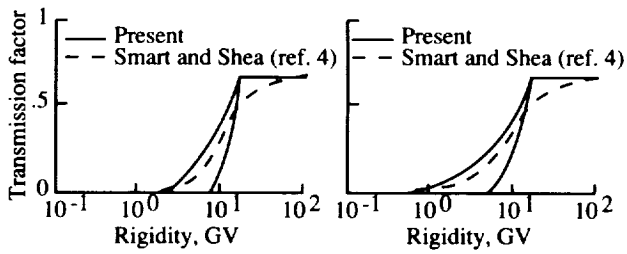

(c) Orbit inclination, 40°. (d) Orbit inclination, 50°.

Figure 1. Dipole maximum and minimum cutoff model and numerical simulation of exact geomagnetic field model.

Geomagnetic Transmission Factor

In arriving at expressions for the geomagnetic transmission factors, the following assumptions are made:

1. Solar cosmic rays are isotropic
2. No transmission below the vertical cutoff (ref. 2) energy
3. Transmission above the vertical cutoff is limited only by the Earth's shadow
4. The geomagnetic field is a tilted dipole field with magnetic north at 79° north and 70° west
5. For mathematical convenience, the geomagnetic storm field is a uniform field H_{st} parallel to the geomagnetic dipole moment (ref. 2)
6. The spacecraft is in a low-altitude circular orbit of arbitrary inclination

Under assumptions 1, 2, 3, and 6, the transmission at fixed geomagnetic latitude λ_m is

$$F_v(R, \lambda_m) = U\left[R - R_c(\lambda_m)\right] \Omega_{\text{sh}} \tag{1}$$

where $U(x)$ is the unit step function, R is the particle rigidity (momentum per unit charge), $R_c(\lambda_m)$ is the vertical cutoff rigidity at λ_m, and

$$\Omega_{\text{sh}} = \frac{1}{2}\left[1 + \cos\left(\sin^{-1}\frac{1}{r}\right)\right] \tag{2}$$

where r is the orbit radius in units of Earth radii. Assumption 4 provides a relationship between magnetic latitude λ_m and geographic coordinates (λ_g, ϕ_g) as

$$\begin{aligned}\sin\lambda_m &= \sin\lambda_g \cos 11^\circ \\ &\quad + \cos\lambda_g \sin 11^\circ \cos\left(\phi_g + 70^\circ\right)\end{aligned} \tag{3}$$

where λ_g, ϕ_g are known functions of time given the orbital parameters (ref. 3). Assumption 6 allows the vertical cutoff to be obtained (ref. 2) as

$$R_c(\lambda_m) = \frac{14.9}{r^2}\cos^4\lambda_m \tag{4}$$

The peak intensity of many solar cosmic ray events lasts for a few to several hours so that only one or at most several orbits will be executed during the main event duration. The maximum exposure occurs when the spacecraft orbit lies closest to the magnetic poles. Since the line of nodes advances 22° every 1½ hours, the minimum exposed orbit occurs 12 hours later. In estimating space exposure, it is critical to know the relative location of the spacecraft in relation to the magnetic poles. Without such specific information, we will evaluate the geomagnetic transmission factors averaged over the orbit with maximum exposure and minimum exposure as a guide to defining action levels where a more complete assessment must be done or specific mission-related considerations are to be made.

The orbit average transmission is given by

$$\overline{F}(R, i) = \frac{\Omega_{\text{sh}}}{T}\int_0^T U\left\{R - R_c[\lambda_m(t)]\right\} dt \tag{5}$$

where T is the time in orbit, $\lambda_m(t)$ is the time-dependent trajectory over the magnetic latitude, and i is orbit inclination.

As the orbit precesses around the Earth's equator, the dose per orbit for a fixed environment goes through a maximum exposed orbit and a minimum exposed orbit. If the inclination angle is less than 79°, then the magnetic latitude is always less than 90°. On a given orbit, the average transmission factor is

$$\begin{aligned}\overline{F}_{\max}(R, i) &= \frac{\Omega_{\text{sh}}}{i + \theta_m}\int_0^{i+\theta_m} U\left[R - R_c(\lambda)\right] d\lambda \\ &= \frac{i + \theta_m - \lambda_m}{i + \theta_m}\Omega_{\text{sh}}\end{aligned} \tag{6}$$

where θ_m is the tilt angle of the magnetic pole ($\theta_m = 11^\circ$) and λ_m is the magnetic latitude with cutoff at R

$$R_c(\lambda_m) = R \tag{7}$$

If i is greater than 79°, then the maximum orbit will always pass over the magnetic pole such that

$$\begin{aligned}\overline{F}_{\max}(R, i) &= \frac{2\Omega_{\text{sh}}}{\pi}\int_0^{\pi/2} U\left[R - R_c(\lambda)\right] d\lambda \\ &= \frac{2}{\pi}\left(\frac{\pi}{2} - \lambda_m\right)\Omega_{\text{sh}}\end{aligned} \tag{8}$$

Similarly, the minimum exposed orbit is

$$\begin{aligned}\overline{F}_{\min}(R, i) &= \frac{\Omega_{\text{sh}}}{i - \theta_m}\int_0^{i-\theta_m} U\left[R - R_c(\lambda)\right] d\lambda \\ &= \frac{1}{i - \theta_m}\left(i - \theta_m - \lambda_m\right)\Omega_{\text{sh}}\end{aligned} \tag{9}$$

whenever $\frac{\pi}{2} \geq i > \theta_m$. Otherwise

$$\begin{aligned}\overline{F}_{\min}(R, i) &= \frac{\Omega_{\text{sh}}}{\theta_m - i}\int_0^{\theta_m - i} U\left[R - R_c(\lambda)\right] d\lambda \\ &= \frac{1}{\theta_m - i}\left(\theta_m - i - \lambda_m\right)\Omega_{\text{sh}}\end{aligned} \tag{10}$$

whenever $i < \theta_m$. The maximum and minimum geomagnetic transmission factors are shown in figure 1 with the orbit-averaged transmission factors for which the angular dependence of direction of arrival at orbit is fully accounted for by Smart and Shea (ref. 4). Even in this simplified model, the average transmission factor for the worst exposed orbit lies well above the long-term average transmission calculated by Smart and Shea as shown in figure 1.

During times of intense solar activity, the solar plasma emitted in solar flares and subflares advances outward and arrives at 1 AU from the Sun. If the Earth is locally present, the plasma interacts with the geomagnetic field in which the plasma pressure performs work on the local geomagnetic field. The plasma flow generates large electric currents and a corresponding impressed magnetic storm field. In the initial phase, the storm field is parallel to the quiet equatorial field, then in the main phase of the storm,

the storm field reverses and opposes the quiet field; this causes a net decrease in the field strength. The main phase is followed by slow recovery to the quiet field conditions.

The magnetic storm model is represented by a uniform magnetic field that is impressed on the normal quiet field. The storm field strength is found from the change in the horizontal field component around the geomagnetic equator. We represent this field by H_{st}. Typical values of H_{st} in the main phase range from 100 nT to 800 nT for a severe magnetic storm corresponding to a range of planetary magnetic index K_p from 5 to 9. The vertical cutoff rigidities are modified due to the presence of the storm field as

$$R_c(\lambda_m) = \frac{14.9}{r^2}\cos^4\lambda_m\left[1 + \frac{H_{st}r^3}{M}\left(\frac{4}{\cos^6\lambda_m} - 1\right)\right] \quad (11)$$

where M is the Earth's magnetic dipole moment. Note that negative values of equation (11) are taken as a zero cutoff. With the exception of this modification of the main field, the results of equations (5) through (9) are applicable for evaluating the transmission factors.

Buildup Factors

In passing through tissue, energetic protons interact mostly through ionization of atomic constituents by the transfer of small amounts of momentum to orbital electrons. Although the nuclear reactions are far less numerous, their effects are magnified because of the large momentum transferred to the nuclear particles and the struck nucleus itself. Unlike the secondary electrons formed through atomic ionization by interaction with the primary protons, the radiations resulting from nuclear reactions are mostly heavily ionizing and generally have large biological effectiveness. Many of the secondary particles of nuclear reactions are sufficiently energetic to promote similar nuclear reactions and thus cause a buildup of secondary radiations. The description of such processes requires a solution of the transport equation. The approximate solutions for the transport of protons in 30-cm-thick slabs of soft tissue for fixed incident energies have been made (refs. 5 through 12). The results of such calculations are dose conversion factors for relating the primary monoenergetic proton fluence to dose or dose equivalent as a function of position in a tissue slab.

Whenever the radiation is spatially uniform, the dose at any point x in a convex object may be calculated (ref. 13) by

$$D(x) = \int_0^\infty \int_\Omega R_n\left[z_x(\Omega), E\right]\phi(\Omega, E)\, d\Omega\, dE \quad (12)$$

where $R_n(z,E)$ is the dose at depth z for normal incident protons of energy E on a tissue slab, $\phi(\Omega, E)$ is the differential proton fluence as modified by the geomagnetic transmission along direction Ω, and $z_x(\Omega)$ is the distance from the boundary along Ω to the point x. It has been shown that equation (12) always overestimates the dose but is an accurate estimate when the ratio of the proton beam divergence due to nuclear reaction to the body's radius of curvature is small. Equation (12) is a practical prescription for introducing nuclear reaction effects into calculations of dose in geometrically complex objects, such as the human body. The main requirement is that the dose conversion factors for a tissue slab be adequately known for a broad range of energies and depths.

Available information on conversion factors is for discrete energies from 100 MeV to 1 TeV in rather broad energy steps and for depths from 0 to 30 cm in semi-infinite slabs of tissue (refs. 5, 7, 9, and 12). The nuclear reaction data used for high-energy nucleons are usually based on Monte Carlo (refs. 14 through 16) estimates with low-energy neutron reaction data taken from experimental observation. The quality factor as defined by the ICRP (ref. 17) is used for protons. The quality factor for heavier fragments and the recoiling nuclei is arbitrarily set to 20 which is considered conservative, but the average quality factor obtained by calculation is comparable with estimates obtained through observations made in nuclear emulsion (ref. 18).

To fully utilize equation (12), a parameterization of the conversion factors was introduced by Wilson and Khandelwal (ref. 13) which allowed reliable interpolation and extrapolation from known values. A refinement and extension of that work is now discussed.

The conversion factor $R_n(z,E)$ is composed of two terms representing dose due to the primary beam protons and the dose due to secondary particles produced in nuclear reaction. Thus,

$$R_n(z,E) = R_p(z,E) + R_s(z,E) \quad (13)$$

where the primary dose equivalent conversion factor is

$$R_p(z,E) = \frac{P(E)\, Q_F\left[S(E_r)\right] S(E_r)}{P(E_r)} \quad (14)$$

with the reduced energy given by

$$E_r = \varepsilon\left[R(E) - z\right] \quad (15)$$

with the usual quality factor Q_F defined as a function of linear energy transfer (LET), with LET denoted

here by the symbol S, and total nuclear survival probability for a proton of energy E given by

$$P(E) = \exp\left[-\int_0^E \frac{\sigma(E')\,dE'}{S(E')}\right] \qquad (16)$$

where the macroscopic cross section $\sigma(E)$ for tissue as calculated by Bertini is given by Alsmiller et al. (ref. 19). The $R(E)$ is the usual range-energy relation for protons in tissue and $\varepsilon(x)$ is the inverse of $R(E)$. The proton total optical thickness given by

$$\tau(E) = \int_0^E \frac{\sigma(E')\,dE'}{S(E')} \qquad (17)$$

is tabulated in table 1 for purposes of numerical interpolation. In the case of conversion factors for absorbed dose, $R_p(z,E)$ is taken as

$$R_p(z,E) = \frac{P(E)\;S(E_r)}{P(E_r)} \qquad (18)$$

The representation of the conversion factors is simplified (ref. 13) by rewriting equation (11) as

$$R_n(z,E) = \left[1 + \frac{R_s(z,E)}{R_p(z,E)}\right] R_p(z,E)$$

$$\equiv B(z,E)\;R_p(z,E) \qquad (19)$$

where $B(z,E)$ is recognized as the dose buildup factor. The main advantage of introducing the buildup factor into equation (19) is that unlike $R_n(z,E)$, the buildup factor is a smoothly varying function of energy at all depths in the slab and can be approximated by the simple function (ref. 13)

$$B(z,E) = (A_1 + A_2 z + A_3 z^2)\exp(-A_4 z) \qquad (20)$$

where the parameters A_i are understood to be energy dependent. The parameters A_i are found by fitting equation (20) to the values of the buildup factors as estimated from the Monte Carlo calculations of proton conversion factors. The resulting coefficients are shown in table 2. The coefficients for 100-, 200-, and 300-MeV protons were obtained with the Monte Carlo data of Turner et al. (ref. 9). The values at 400, 730, 1500, and 3000 MeV were obtained from the results of Alsmiller, Armstrong, and Coleman (ref. 5). The 10-GeV entry was obtained from the calculations of Armstrong and Chandler (ref. 7). Values noted in table 2 by an asterisk on the corresponding energy were obtained by interpolating between data points or smoothly extrapolating to unit buildup factor at proton energies near the Coulomb barrier for tissue nuclei (≈12 MeV). The coefficients are found for all energies to 10 GeV by using second order Lagrange interpolation between the values shown in table 2. The resulting buildup factors are shown in figures 2 and 3 in comparison to the Monte Carlo results where the error bars were determined by drawing smooth limiting curves so as to bracket the Monte Carlo values and to follow the general functional dependence. These uncertainty limits should, therefore, be interpreted as approximately 2σ limits, rather than 1σ ranges usually used in expressing uncertainty limits.

Table 1. Total Tissue Optical Thickness for Protons

E, GeV	$\tau\,(E)$	E, GeV	$\tau\,(E)$
0	0	1.3	6.57
.01	.0033	1.5	8.03
.025	.0171	1.7	9.52
.05	.0510	2.0	11.76
.1	.135	2.2	13.27
.15	.239	2.4	14.78
.2	.362	2.6	16.29
.25	.501	2.8	17.79
.3	.655	3.0	19.29
.35	.822	4.0	26.62
.4	1.004	5.0	33.81
.5	1.429	6.0	40.84
.7	2.471	7.0	47.75
.9	3.743	8.5	57.91
1.1	5.143	10.0	67.85

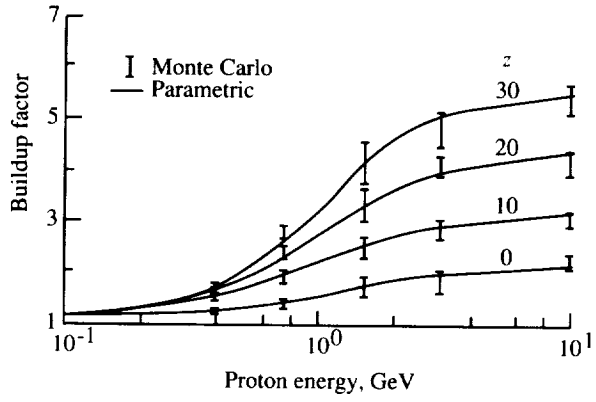

Figure 2. Dose buildup factor for several depths in tissue as function of incident proton energy.

Table 2. Buildup Factor Parameters

	Dose equivalent				Dose			
E, GeV	A_1	A_2	A_3	A_4	A_1	A_2	A_3	A_4
*0.03	1.00	0	0	0	1.00	0	0	0
*.06	1.20	0	0	.0130	1.07	.010	0	.010
.10	1.40	.020	0	.0300	1.10	.040	0	.026
*.15	1.50	.070	0	.0385	1.12	.060	0	.031
.20	1.60	.090	0	.0400	1.15	.062	0	.032
.30	1.70	.110	0	.0330	1.20	.068	0	.026
.40	1.90	.130	0	.0228	1.24	.071	0	.0228
.73	3.40	.156	.00035	.0150	1.40	.090	.0001	.0150
*1.2	4.32	.167	.00145	.0130	1.67	.094	.0008	.0122
1.5	4.60	.170	.00250	.0120	1.80	.095	.0015	.0120
3.0	5.35	.190	.00300	.0100	2.00	.100	.0020	.0100
10.0	6.20	.280	.00350	.0100	2.30	.111	.00205	.0100

*Interpolated values.

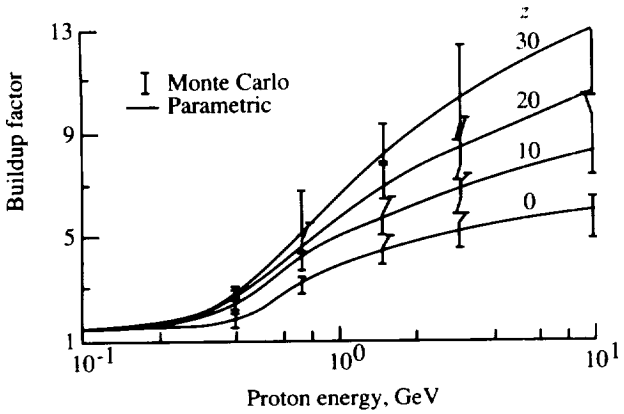

Figure 3. Dose equivalent buildup factor for several depths in tissue as function of incident proton energy.

The dose as a function of depth is shown in comparison to measurements of Baarli and Goebel at CERN (Switzerland) in figure 4. Also shown are the Monte Carlo values interpolated between 400 and 730 MeV. The uncollided primary proton contribution is shown separately. The dose equivalent is likewise shown in figure 5. The extreme importance of secondary radiation is clearly shown.

Within the space program, one has shield material which is mostly aluminum. We are therefore interested in the attenuation of the space radiation by the appropriate amount of aluminum before entering the astronaut's body. As a first step, we replace the appropriate aluminum thickness z_s (g/cm^2) by a range of equivalent thickness of tissue $\hat{z}_s$ for 50-MeV protons as has been the custom in space radiation protection as

$$\hat{z}_s = \frac{R_{\text{tiss}}(50)}{R_{\text{Al}}(50)} z_s \equiv \rho z_s \tag{21}$$

The primary dose equivalent conversion factor is then

$$R_p(z+\hat{z}_s,E) = \exp\left[-\left(\rho^{-1}\sigma_{\text{Al}} - \sigma_{\text{tiss}}\right)\hat{z}_s\right] \times \frac{P(E)\; Q_F\left[S(E_r)\right] S(E_r)}{P(E_r)} \tag{22}$$

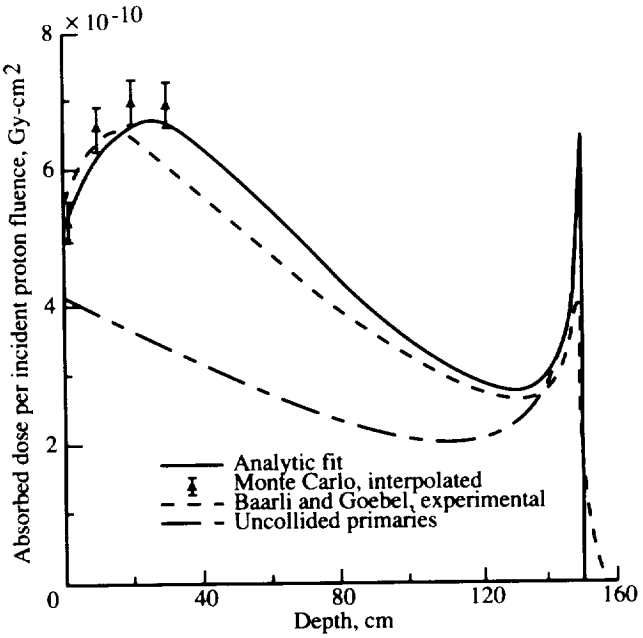

Figure 4. Proton depth-dose relation: analytic fit (nuclear effects), experiments and Monte Carlo, experiments and from primary protons. 592-MeV protons.

where the reduced energy is

$$E_r = \varepsilon\left[R(E) - z - \hat{z}_s\right] \tag{23}$$

and the exponential factor corrects $P(E)$ by the appropriate aluminum-tissue combined attenuation factor. The primary absorbed dose is identical in form to equation (22) except that $Q_F(S)$ is equal to unity. Note σ_{Al} and σ_{tiss} are taken as the asymptotic macroscopic cross sections where energy dependence is negligible. The complete conversion factors are

$$R_n(z+\hat{z}_s,E) = R_p(z+\hat{z}_s,E) + R_s(z+\hat{z}_s,E) \tag{24}$$

where $R_s(z+\hat{z}_s,E)$ is the contribution including secondary particles. We rewrite equation (24) as

$$R_n(\hat{z}_s,z,E) = B_\Delta(\hat{z}_s,E)\; R_{\text{tiss}}(z+\hat{z}_s,E) \tag{25}$$

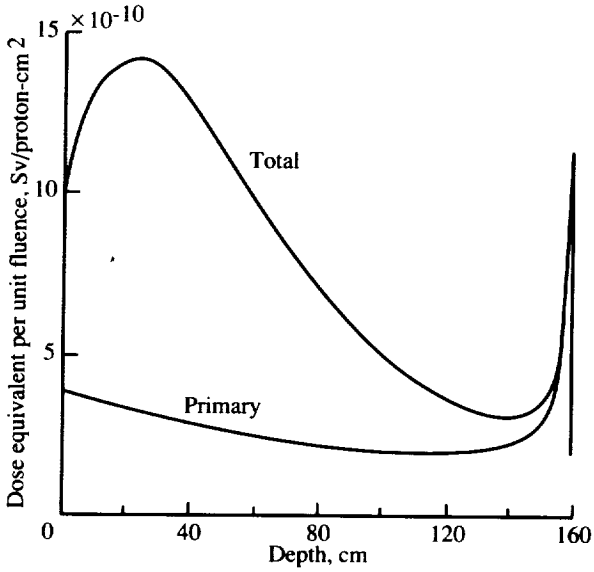

Figure 5. Proton depth-dose equivalent relation including nuclear effects. 600-MeV protons.

where $B_\Delta(\hat{z}_s,E)$ is an aluminum buildup factor relative to tissue which is unity for $\hat{z}_s = 0$ and $E << 100$ MeV. The aluminum factor has been found (units for E are GeV and for $\hat{z}_s$ are g/cm^2) to be reasonably approximated by

$$B_\Delta(\hat{z}_s,E) = 1 + \frac{0.02\hat{z}_s E}{1+E} e^{-0.022\hat{z}_s} \qquad (26)$$

for dose equivalent and

$$B_\Delta(\hat{z}_s,E) = 1 + \frac{0.02\hat{z}_s E}{6(1+E)} e^{-0.01\hat{z}_s} \qquad (27)$$

for absorbed dose. Equation (10) is rewritten as

$$D(x) = \int_0^\infty \int_\Omega R_n\,[\hat{z}_s(\Omega),z(\Omega),E]\,\phi(\Omega,E)\,d\Omega\,dE \qquad (28)$$

where $\hat{z}_s(\Omega)$ is the aluminum thickness distribution about the dose point x and $z(\Omega)$ is the astronaut self-shielding distribution about the dose point (ref. 20).

The exposure limits proposed for Space Station Freedom (ref. 21) are shown in table 3. For any particular environment the shield design must maintain exposure below these values.

Results and Discussion

Sample calculations are made for three solar events of Solar Cycles 19 and 20. The spectra for these three events are shown in figure 6. The February 1956 event was an event for which the most energetic particles arrived in about a 2-hour time period. The dose and dose equivalent within a 1, 3, and 5 g/cm^2 aluminum spherical shell for critical body organs are shown in tables 4, 5, 6, and 7 in which the vehicle is in a maximum exposed 400-km circular orbit of various inclinations and a minimum exposed 400-km circular orbit of various inclinations, respectively. Also shown are results for the November 1960 and August 1972 events which were of longer duration for which the average between the maximum and minimum orbits would be more indicative of the actual exposure.

Table 3. Ionizing Radiation Exposure Limits for Space Station Freedom Astronauts

Exposure interval	Dose equivalent, cSv, for—		
	Skin	Eye	Blood-forming organs
30 days	150	100	25
Annual	300	200	50
Career	600	400	[a]100–400

[a]Dependent on gender and age at initial exposure.

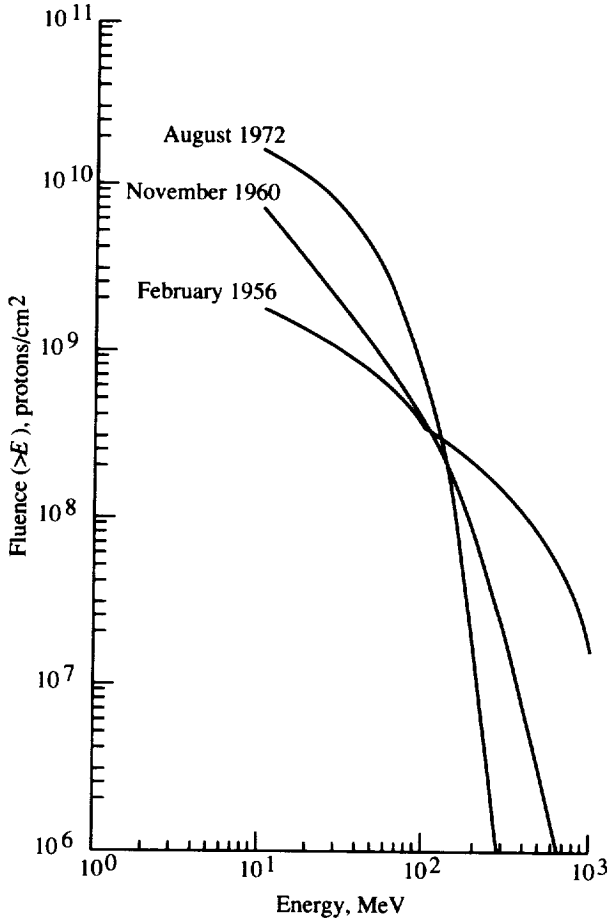

Figure 6. Proton fluence of three major solar events.

The maximum permissible exposure limits for the current space program are shown in table 3. The skin dose in table 4 is indicative of the onboard dosimeters. The skin dose equivalents of table 5 are to be maintained within 150 cSv within any 1-month period. Since the typical spacecraft wall is about 1 g/cm^2 of aluminum, a flare shelter must be provided for orbits of inclination above 60° if the geomagnetic field is quiet. Similar shielding is required to adequately shield the blood-forming organs (BFO) during quiet field times. The ocular lens dose and dose equivalent are within 10 percent of the skin exposure values. Clearly, a shelter with more than 3 g/cm^2 of aluminum must be provided to maintain ocular lens exposures below current limits in table 3.

An additional factor is the effect of a geomagnetic disturbance which can greatly alter the cutoff values used in the quiet time model. Such disturbances are common because of the increased plasma output from the Sun during solar flares. Since the initial phase of a magnetic storm reduces the transmission to below quiet time values, we will look at results during the main phase only. The exposure of the skin and the BFO are shown for the three-event spectra in figure 6 and during a severe magnetic storm in tables 8 through 11. The typical spacecraft wall is very inefficient in protecting the skin in the high inclined orbits with some possibility of erythema in the most sensitive individuals. A flare shelter of 5 g/cm^2 or more would be considered adequate for inclinations above 70°. Such a shelter appears to be adequate for the BFO provided the cumulative exposure of other sources is minimal.

NASA Langley Research Center
Hampton, VA 23665-5225
April 13, 1990

Table 4. Skin Dose Behind Aluminum Shield During February 25, 1956, November 12–13, 1960, and August 4, 1972, Events

Orbit inclination, deg	Skin dose, cGy, during—								
	Feb. 1956 for z_s, g/cm^2, of—			Nov. 1960 for z_s, g/cm^2, of—			Aug. 1972 for z_s, g/cm^2, of—		
	1	3	5	1	3	5	1	3	5
30, max	0	0	0	0	0	0	0	0	0
30, min	0	0	0	0	0	0	0	0	0
40, max	<0.1	<0.1	<0.1	0	0	0	0	0	0
40, min	0	0	0	0	0	0	0	0	0
50, max	0.5	0.5	0.5	<0.1	<0.1	0.1	<0.1	<0.1	<0.1
50, min	<0.1	<0.1	<0.1	0	0	0	0	0	0
60, max	7.1	4.9	3.9	16.0	7.0	5.0	49.0	25.0	14.0
60, min	<0.1	<0.1	<0.1	0	0	0	0	0	0
70, max	19.0	5.7	7.4	51.0	71.0	11.0	160.0	64.0	33.1
70, min	0.3	0.3	0.3	<0.1	<0.1	0.1	<0.1	<0.1	<0.1
80, max	27.0	14.0	10.0	76.0	23.0	15.0	230.0	92.0	47.0
80, min	4.3	3.6	3.1	7.6	4.8	3.7	24.0	16.0	9.7
90, max	27.0	14.0	10.0	76.0	23.0	15.0	230.0	92.0	47.0
90, min	17.0	9.3	6.8	44.0	15.0	9.6	140.0	47.0	30.0

Table 5. Skin Dose Equivalent Behind Aluminum Shield During February 25, 1956, November 12–13, 1960, and August 4, 1972, Events

Orbit inclination, deg	Skin dose equivalent, cSv, during—								
	Feb. 1956 for z_s, g/cm^2, of—			Nov. 1960 for z_s, g/cm^2, of—			Aug. 1972 for z_s, g/cm^2, of—		
	1	3	5	1	3	5	1	3	5
30, max	0	0	0	0	0	0	0	0	0
30, min	0	0	0	0	0	0	0	0	0
40, max	<0.1	<0.1	<0.1	0	0	0	0	0	0
40, min	0	0	0	0	0	0	0	0	0
50, max	1.1	1.1	1.2	0.1	0.1	0.1	<0.1	<0.1	<0.1
50, min	<0.1	0	0	0	0	0	0	0	0
60, max	10.0	7.4	6.2	22.0	8.9	6.4	64.0	30.0	17.0
60, min	0.1	0.1	0.1	0	0	0	0	0	0
70, max	27.0	15.0	11.0	73.0	21.0	13.0	210.0	78.0	40.0
70, min	0.7	0.7	0.7	<0.1	<0.1	<0.1	<0.1	<0.1	0
80, max	39.0	20.0	15.0	110.0	29.0	19.0	320.0	110.0	56.0
80, min	6.5	5.6	5.0	7.6	6.2	4.7	24.0	19.0	9.7
90, max	39.0	20	15.0	110.0	29.0	19.0	320.0	110.0	56.0
90, min	24.0	13	8.1	64.0	19.0	12.0	190.0	70.0	36.0

Table 6. BFO Dose Behind Aluminum Shield During February 25, 1956, November 12–13, 1960, and August 4, 1972, Events

Orbit inclination, deg	BFO dose, cGy, during								
	Feb. 1956 for z_s, g/cm^2, of—			Nov. 1960 for z_s, g/cm^2, of			Aug. 1972 for z_s, g/cm^2, of		
	1	3	5	1	3	5	1	3	5
30, max	0	0	0	0	0	0	0	0	0
30, min	0	0	0	0	0	0	0	0	0
40, max	<0.1	<0.1	<0.1	0	0	0	0	0	0
40, min	0	0	0	0	0	0	0	0	0
50, max	0.5	0.5	0.5	<0.1	<0.1	<0.1	<0.1	<0.1	<0.1
50, min	<0.1	0	0	0	0	0	0	0	0
60, max	3.2	2.9	2.8	3.6	3.1	2.8	7.6	5.0	3.6
60, min	<0.1	<0.1	<0.1	0	0	0	0	0	0
70, max	5.7	5.1	4.7	7.5	6.2	5.4	17.0	11.0	7.5
70, min	0.3	0.3	0.3	<0.1	<0.1	<0.1	<0.1	<0.1	<0.1
80, max	7.5	6.6	6.1	10.0	8.4	7.3	24.0	15.0	10.0
80, min	2.7	2.4	2.3	2.7	2.4	2.2	5.3	3.6	2.6
90, max	7.5	6.6	6.1	10.0	8.4	7.3	24.0	15.0	10.0
90, min	5.3	4.7	4.4	6.8	5.7	5.0	16.0	9.9	6.8

Table 7. BFO Dose Equivalent Behind Aluminum Shield During February 25, 1956, November 12–13, 1960, and August 4, 1972, Events

Orbit inclination, deg	BFO dose equivalent, cSv, during—								
	Feb. 1956 for z_s, g/cm^2, of—			Nov. 1960 for z_s, g/cm^2, of			Aug. 1972 for z_s, g/cm^2, of—		
	1	3	5	1	3	5	1	3	5
30, max	0	0	0	0	0	0	0	0	0
30, min	0	0	0	0	0	0	0	0	0
40, max	<0.1	<0.1	<0.1	<0.1	<0.1	<0.1	0	0	0
40, min	0	0	0	0	0	0	0	0	0
50, max	1.1	1.2	1.2	0.1	0.1	0.1	<0.1	<0.1	<0.1
50, min	<0.1	0	0	0	0	0	0	0	0
60, max	5.4	5.1	4.9	5.1	4.4	4.0	11.0	7.0	5.4
60, min	<0.1	<0.1	<0.1	0	0	0	0	0	0
70, max	9.4	8.5	8.1	11.0	8.6	7.7	15.0	15.0	11.0
70, min	0.7	0.7	0.7	<0.1	<0.1	<0.1	<0.1	<0.1	<0.1
80, max	12.0	11.0	10.0	14.0	12.0	10.0	36.0	21.0	16.0
80, min	4.5	4.3	4.2	3.8	3.4	3.1	7.5	5.0	3.9
90, max	12.0	11.0	10.0	14.0	12.0	10.0	36.0	21.0	16.0
90, min	8.7	7.9	7.5	9.6	7.9	7.1	23.0	14.0	10.0

Table 8. Skin Dose Behind Aluminum Shield During February 25, 1956, November 12–13, 1960, and August 4, 1972, Events With Geomagnetic Storm Conditions (−100 nT)

Orbit inclination, deg	Skin dose, cGy, during—								
	Feb. 1956 for z_s, g/cm^2, of—			Nov. 1960 for z_s, g/cm^2, of—			Aug. 1972 for z_s, g/cm^2, of—		
	1	3	5	1	3	5	1	3	5
30, max	0	0	0	0	0	0	0	0	0
30, min	0	0	0	0	0	0	0	0	0
40, max	<0.1	<0.1	<0.1	0	0	0	0	0	0
40, min	0	0	0	0	0	0	0	0	0
50, max	5.6	3.4	2.6	1.4	5.0	3.34	43.0	18.0	9.9
50, min	<0.1	0	0	0	0	0	0	0	0
60, max	19.0	9.8	6.9	54.0	16.0	10.0	170.0	64.0	32.0
60, min	<0.1	<0.1	<0.1	0	0	0	0	0	0
70, max	30.0	15.0	10.0	84.0	25.0	15.0	260.0	98.0	49.0
70, min	2.3	1.9	1.6	4.2	2.3	1.7	13.0	7.5	4.5
80, max	37.0	18.0	12.0	110.0	30.0	19.0	330.0	120.0	61.0
80, min	17.0	8.7	6.1	47.0	14.0	8.8	150.0	56.0	28.0
90, max	37.0	18.0	12.0	110.0	30.0	19.0	330.0	120.0	61.0
90, min	28.0	14.0	9.5	79.0	23.0	14.0	240.0	92.0	46.0

Table 9. Skin Dose Equivalent Behind Aluminum Shield During February 25, 1956, November 12–13, 1960, and August 4, 1972, Events With Geomagnetic Storm Conditions (−100 nT)

Orbit inclination, deg	Skin dose equivalent, cSv, during—								
	Feb. 1956 for z_s, g/cm^2, of—			Nov. 1960 for z_s, g/cm^2, of—			Aug. 1972 for z_s, g/cm^2, of—		
	1	3	5	1	3	5	1	3	5
30, max	0	0	0	0	0	0	0	0	0
30, min	0	0	0	0	0	0	0	0	0
40, max	0.1	0.1	0.1	0	0	0	0	0	0
40, min	0	0	0	0	0	0	0	0	0
50, max	8.3	5.1	4.2	20.0	6.3	4.3	58.0	23.0	12.0
50, min	0	0	0	0	0	0	0	0	0
60, max	28.0	14.0	10.0	79.0	20.0	13.0	230.0	78.0	39.0
60, min	<0.1	<0.1	<0.1	0	0	0	0	0	0
70, max	42.0	20.0	15.0	120.0	31.0	19.0	360.0	120.0	65.0
70, min	3.6	3.0	2.7	5.8	3.0	2.3	16.0	9.1	5.5
80, max	53.0	25.0	18.0	150.0	38.0	23.0	450.0	150.0	74.0
80, min	24.0	12.0	9.1	69.0	18.0	8.8	200.0	68.0	34.0
90, max	53.0	25.0	18.0	150.0	38.0	23.0	450.0	150.0	74.0
90, min	40.0	19.0	14.0	120.0	29.0	14.0	340.0	110.0	56.0

Table 10. BFO Dose Behind Aluminum Shield During February 25, 1956, November 12–13, 1960, and August 4, 1972, Events With Geomagnetic Storm Conditions (−100 nT)

Orbit inclination, deg	BFO dose, cGy, during—								
	Feb. 1956 for z_s, g/cm^2, of—			Nov. 1960 for z_s, g/cm^2, of—			Aug. 1972 for z_s, g/cm^2, of—		
	1	3	5	1	3	5	1	3	5
30, max	0	0	0	0	0	0	0	0	0
30, min	0	0	0	0	0	0	0	0	0
40, max	<0.1	<0.1	<0.1	0	0	0	0	0	0
40, min	0	0	0	0	0	0	0	0	0
50, max	2.1	1.9	1.8	3.4	2.1	1.8	5.3	3.4	2.4
50, min	0	0	0	0	0	0	0	0	0
60, max	5.2	4.6	4.2	9.9	5.7	5.0	17.0	10.0	7.0
60, min	<0.1	<0.1	<0.1	0	0	0	0	0	0
70, max	12.0	6.5	6.0	15.0	8.5	7.3	26.0	16.0	11.0
70, min	1.4	1.3	1.3	1.3	1.2	1.1	2.5	1.7	1.2
80, max	9.1	7.9	7.2	18.0	10.0	9.0	32.0	20.0	13.0
80, min	4.6	4.1	3.8	6.2	5.1	4.4	15.0	9.2	6.2
90, max	9.1	7.9	7.2	18.0	10.0	9.0	32.0	20.0	13.0
90, min	7.1	6.2	5.6	9.8	8.0	6.9	24.0	15.0	9.9

Table 11. BFO Dose Equivalent Behind Aluminum Shield During February 25, 1956, November 12–13, 1960, and August 4, 1972, Events With Geomagnetic Storm Conditions (−100 nT)

Orbit inclination, deg	BFO dose equivalent, cSv, during—								
	Feb. 1956 for z_s, g/cm^2, of—			Nov. 1960 for z_s, g/cm^2, of—			Aug. 1972 for z_s, g/cm^2, of—		
	1	3	5	1	3	5	1	3	5
30, max	0	0	0	0	0	0	0	0	0
30, min	0	0	0	0	0	0	0	0	0
40, max	0.1	0.1	0.1	0	0	0	0	0	0
40, min	0	0	0	0	0	0	0	0	0
50, max	3.6	3.4	3.3	3.4	2.9	2.6	7.6	4.8	3.6
50, min	0	0	0	0	0	0	0	0	0
60, max	8.5	7.5	7.1	9.9	7.9	7.1	25.0	15.0	11.0
60, min	<0.1	<0.1	<0.1	0	0	0	0	0	0
70, max	12.0	11.0	10.0	15.0	12.0	10.0	37.0	22.0	16.0
70, min	2.5	2.4	2.3	1.9	1.6	1.5	2.5	2.4	1.9
80, max	15.0	13.0	12.0	18.0	14.0	13.0	46.0	28.0	20.0
80, min	7.6	6.8	6.5	8.7	7.0	6.3	22.0	13.0	9.5
90, max	15.0	13.0	12.0	18.0	14.0	13.0	46.0	28.0	20.0
90, min	11.0	10.0	9.5	14.0	11.0	9.8	35.0	21.0	15.0

References

1. Atwell, William; Beaver, E. Ralph; Hardy, Alva C.; and Cash, Bernard L.: A Radiation Shielding Model of the Space Shuttle for Space Radiation Dose Exposure Estimations. *Advances in Nuclear Engineering Computation and Radiation Shielding*, Volume 1, Michael L. Hall, ed., American Nuclear Soc., Inc., c.1989, pp. 11:1–11:12.
2. Kuhn, E.; Schwamb, F. E.; and Payne, W. T.: Solar Flare Hazard to Earth-Orbiting Vehicles. *Second Symposium on Protection Against Radiations in Space,* Arthur Reetz, Jr., ed., NASA SP-71, 1965, pp. 429–434.
3. Wilson, John W.; and Denn, Fred M.: *Implications of Outer Zone Radiations on Operations in the Geostationary Region Utilizing the AE4 Environmental Model.* NASA TN D-8416, 1977.
4. Smart, D. F.; and Shea, M. A.: Geomagnetic Transmission Functions for a 400 km Altitude Satellite. *18th International Cosmic Ray Conference—Conference Papers,* MG Sessions, Volume 3, Tata Inst. of Fundamental Research (Colaba, Bombay), 1983, pp. 419–422.
5. Alsmiller, R. G., Jr.; Armstrong, T. W.; and Coleman, W. A.: The Absorbed Dose and Dose Equivalent From Neutrons in the Energy Range 60 to 3000 MeV and Protons in the Energy Range 400 to 3000 MeV. *Nucl. Sci. & Eng.*, vol. 42, no. 3, Dec. 1970, pp. 367–381.
6. Armstrong, T. W.; and Bishop, B. L.: Calculation of the Absorbed Dose and Dose Equivalent Induced by Medium-Energy Neutrons and Protons and Comparison With Experiment. *Radiat. Res.*, vol. 47, no. 3, Sept. 1971, pp. 581–588.
7. Armstrong, T. W.; and Chandler, K. C.: *Calculation of the Absorbed Dose and Dose Equivalent From Neutrons and Protons in the Energy Range From 3.5 GeV to 1.0 TeV.* ORNL-TM-3758, U.S. Atomic Energy Commission, May 1970.
8. Snyder, W. S.; Wright, H. A.; Turner, J. E.; and Neufeld, Jacob: Calculations of Depth-Dose Curves for High-Energy Neutrons and Protons and Their Interpretation for Radiation Protection. *Nucl. Appl.*, vol. 6, no. 4, Apr. 1969, pp. 336–343.
9. Turner, J. E.; Zerby, C. D.; Woodyard, R. L.; Wright, H. A.; Kinney, W. E.; Synder, W. S.; and Neufeld, J.: Calculation of Radiation Dose From Protons to 400 MeV. *Health Phys.*, vol. 10, no. 11, Nov. 1964, pp. 783–808.
10. Wright, H. A.; Hamm, R. N.; and Turner, J. E.: Effect of Lateral Scattering on Absorbed Dose From 400 MeV Neutrons and Protons. *International Congress on Protection Against Accelerator and Space Radiation,* J. Baarli and J. Dutrannois, eds., CERN 71-16, Vol. 1, European Organization for Nuclear Research, July 1, 1971, pp. 207–219.
11. Wright, Harvel A.; Anderson, V. E.; Turner, J. E.; Neufeld, Jacob; and Snyder, W. S.: Calculation of Radiation Dose Due to Protons and Neutrons With Energies From 0.4 to 2.4 GeV. *Health Phys.*, vol. 16, no. 1, Jan. 1969, pp. 13–31.
12. Zerby, C. D.; and Kinney, W. E.: Calculated Tissue Current-to-Dose Conversion Factors for Nucleons Below 400 MeV. *Nucl. Instrum. & Methods,* vol. 36, no. 1, Sept. 1965, pp. 125–140.
13. Wilson, John W.; and Khandelwal, G. S.: Proton Dose Approximation in Arbitrary Convex Geometry. *Nucl. Technol.*, vol. 23, no. 3, Sept. 1974, pp. 298–305.
14. Bertini, Hugo W.: Low-Energy Intranuclear Cascade Calculation. *Phys. Rev.*, Second ser., vol. 131, no. 4, Aug. 15, 1963, pp. 1801–1821.
15. Bertini, Hugo W.: Intranuclear-Cascade Calculation of the Secondary Nucleon Spectra From Nucleon-Nucleus Interactions in the Energy Range 340 to 2900 MeV and Comparisons With Experiment. *Phys. Review,* second ser., vol. 188, no. 4, Dec. 20, 1969, pp. 1711–1730.
16. Bertini, Hugo W.; and Guthrie, Miriam P.: News Item—Results From Medium-Energy Intranuclear-Cascade Calculation. *Nucl. Phys.*, vol. A169, no. 3, July 1971, pp. 670–672.
17. *Recommendations of the International Commission on Radiological Protection.* ICRP Publ. 26, Pergamon Press, Jan. 17, 1977.
18. Schaefer, Hermann J.; and Sullivan, Jeremiah J.: *Nuclear Emulsion Recordings of the Astronauts' Radiation Exposure on the First Lunar Landing Mission Apollo XI.* NASA CR-115804, 1970.
19. Alsmiller, R. G., Jr.; Santoro, R. T.; Barish, J.; and Claiborne, H. C.: *Shielding of Manned Space Vehicles Against Protons and Alpha Particles.* ORNL-RSIC-35, U.S. Atomic Energy Commission, Nov. 1972.
20. Billings, M. P.; and Yucker, W. R.: *The Computerized Anatomical Man (CAM) Model.* NASA CR-134043, 1973.
21. *Space Station Program Definition and Requirements, Section 3: Space Station Systems Requirements.* SSP 30000, Section 3, Revision F, Space Station Program Off., May 6, 1988.

NASA
National Aeronautics and Space Administration

Report Documentation Page

1. Report No.	2. Government Accession No.	3. Recipient's Catalog No.
NASA TM-4182		

4. Title and Subtitle	5. Report Date
Simplified Model for Solar Cosmic Ray Exposure in Manned Earth Orbital Flights	May 1990
	6. Performing Organization Code
7. Author(s)	8. Performing Organization Report No.
John W. Wilson, Govind S. Khandelwal, Judy L. Shinn, John E. Nealy, Lawrence W. Townsend, and Francis A. Cucinotta	L-16738
9. Performing Organization Name and Address	10. Work Unit No.
NASA Langley Research Center Hampton, VA 23665-5225	199-22-76-01
	11. Contract or Grant No.
12. Sponsoring Agency Name and Address	13. Type of Report and Period Covered
National Aeronautics and Space Administration Washington, DC 20546-0001	Technical Memorandum
	14. Sponsoring Agency Code

15. Supplementary Notes

John W. Wilson, Judy L. Shinn, John E. Nealy, and Lawrence W. Townsend: Langley Research Center, Hampton, Virginia.
Govind S. Khandelwal: Old Dominion University, Norfolk, Virginia.
Francis A. Cucinotta: Rockwell International, Space Transportation Systems Division, Houston, Texas.

16. Abstract

A simple calculational model is derived for use in estimating solar cosmic ray exposure to critical body organs in low Earth orbit at the center of a large spherical shield of fixed thickness. The effects of the Earth's geomagnetic field, including storm conditions and the astronauts' self-shielding, are evaluated explicitly. The magnetic storm model is keyed to the planetary magnetic index K_p.

17. Key Words (Suggested by Authors(s))	18. Distribution Statement
Solar flares Geomagnetism Dose equivalent Nuclear reactions	Unclassified—Unlimited Subject Category 93

19. Security Classif. (of this report)	20. Security Classif. (of this page)	21. No. of Pages	22. Price
Unclassified	Unclassified	13	A03

NASA FORM 1626 OCT 86 NASA-Langley, 1990

For sale by the National Technical Information Service, Springfield, Virginia 22161-2171